Probing the negative permittivity perfect lens at optical frequencies using near-field optics and single molecule detection

Robert J. Moerland and Niek F. van Hulst
University of Twente, Optical Techniques,
P.O. Box 217, 7500 AE Enschede, The Netherlands
r.moerland@utwente.nl

Henkjan Gersen
Interdisciplinary Nanoscience Center (iNANO), Center for Atomic-scale Materials Physics (CAMP), and Department of Physics and Astronomy
University of Aarhus, DK 8000 Aarhus C, Denmark

Laurens Kuipers
FOM Institute for Atomic and Molecular Physics (AMOLF)
Kruislaan 407, 1098 SJ, Amsterdam, The Netherlands

Abstract: Recently, the existence of a perfect lens has been predicted, made of an artificial material that has a negative electric permittivity and a negative magnetic permeability. For optical frequencies a *poormans* version is predicted to exist in the sub-wavelength limit. Then, only the permittivity has to be negative, a demand that metals fulfill at optical frequencies. We propose a new measurement scheme to verify the performance of such a negative permittivity near-perfect lens at optical frequencies. The scheme is based on near-field scanning optical microscopy and single molecule detection. Prerequisite near-field single molecule data, necessary to assess the performance of the lens, is presented. A numerical evaluation, which includes absorption, of the expected performance of a slab of a realistic negative permittivity material confirms the merits of the scheme.

OCIS codes: (260.3910) Metals, optics of; (180.0180) Microscopy; (240.6680) Surface plasmons; (100.6640) Superresolution

References and links

1. J. B. Pendry, "Negative refraction makes a perfect lens," Phys. Rev. Lett. **85**, 3966–3969 (2000).
2. V. G. Veselago, "The electrodynamics of substances with simultaneously negative values of ε and μ," Sov. Phys. Usp. **10**, 509–514 (1968).
3. R. A. Shelby, D. R. Smith, and S. Schultz, "Experimental verification of a negative index of refraction," Science **292**, 77–79 (2001).
4. X. S. Rao and C. K. Ong, "Subwavelength imaging by a left-handed material superlens," Phys. Rev. E **68**, 067601 (2003).
5. X. S. Rao and C. K. Ong, "Amplification of evanescent waves in a lossy left-handed material slab," Phys. Rev. B **68**, 113103 (2003).
6. N. C. Panoiu and R. M. Osgood, "Numerical investigation of negative refractive index metamaterials at infrared and optical frequencies," Opt. Commun. **223**, 331–337 (2003).

#6119 - $15.00 US Received 22 December 2004; revised 23 February 2005; accepted 23 February 2005

7. P. G. Kik, S. A. Maier, and H. A. Atwater, "Image resolution of surface-plasmon-mediated near-field focusing with planar metal films in three dimensions using finite-linewidth dipole sources," Phys. Rev. B **69**, 045418 (2004).
8. D. O. S. Melville, R. J. Blaikie, and C. R. Wolf, "Submicron imaging with a planar silver lens," Appl. Phys. Lett. **84**, 4403–4405 (2004).
9. N. Fang, Z. W. Liu, T. J. Yen, and X. Zhang, "Regenerating evanescent waves from a silver superlens," Opt. Express **11**, 682–687 (2003), http://www.opticsexpress.org/abstract.cfm?URI=OPEX-11-7-682.
10. J. A. Veerman, A. M. Otter, L. Kuipers, and N. F. van Hulst, "High definition aperture probes for near-field optical microscopy fabricated by focused ion beam milling," Appl. Phys. Lett. **72**, 3115–3117 (1998).
11. M. L. M. Balistreri, J. P. Korterik, L. Kuipers, and N. F. van Hulst, "Photon scanning tunneling optical microscopy with a three-dimensional multiheight imaging mode," Appl. Phys. Lett. **77**, 4092–4094 (2000).
12. J. A. Veerman, M. F. Garcia-Parajo, L. Kuipers, and N. F. V. Hulst, "Single molecule mapping of the optical field distribution of probes for near-field microscopy," J. Microscopy-Oxford **194**, 477–482 (1999).
13. N. F. van Hulst, J. A. Veerman, M. F. Garcia-Parajo, and L. Kuipers, "Analysis of individual (macro)molecules and proteins using near-field optics," J. Chem. Phys. **112**, 7799–7810 (2000).
14. B. Sick, B. Hecht, U. P. Wild, and L. Novotny, "Probing confined fields with single molecules and vice versa," J. Microscopy-Oxford **202**, 365–373 (2001).
15. H. Bethe, "Theory of Diffraction by Small Holes," Phys. Rev. **66**, 163 (1944).
16. C. J. Bouwkamp, "On Bethe's theory of diffraction by small holes," Philips Res. Rep. **5**, 321–332 (1950).
17. O. J. F. Martin and M. Paulus, "Influence of metal roughness on the near-field generated by an aperture/apertureless probe," J. Microscopy-Oxford **205**, 147–152 (2002).
18. Computer Simulation Technology, URL http://www.cst.com.
19. D. E. Gray, ed., *American Institute of Physics Handbook*, 3rd ed. (McGraw-Hill Book Company, 1972).
20. S. A. Ramakrishna and J. B. Pendry, "The asymmetric lossy near-perfect lens," J. Modern Opt. **49**, 1747–1762 (2002).

1. Introduction

Since the prediction of the existence of a perfect lens by Pendry in PRL [1], the scientific community has picked up the challenge to prove the expected focusing and amplification of evanescent electromagnetic waves by a slab of left handed material (LHM). In a left handed material both the relative electric permittivity ε as well as the relative magnetic permeability μ are negative. Already in 1968, Veselago showed that such a LHM slab would refract electromagnetic waves 'the other way around', reversing Snell's law [2]. This reversal of the law of refraction allows one to use a planar LHM slab to focus propagating waves and hence be used as a substitute for a positive lens. The resolution of the image formed by a conventional positive lens is governed by the diffraction limit, as only propagating waves coming from an object are focused. The evanescent waves, present in the near field of the object and which contain information on the high spatial frequency components of the object, decay exponentially with distance from the object. This can be understood from a Fourier decomposition of the electric field coming from an object into plane waves:

$$\vec{E}(x,y,z,t) = \sum_{k_x,k_y} \vec{E}(k_x,k_y)\exp(ik_z z + ik_x x + ik_y y - i\omega t). \tag{1}$$

Here, k_x and k_y are the spatial frequencies in the x and y direction respectively and ω is the frequency of the light. Furthermore, k_x, k_y and k_z are coupled:

$$k_z = \sqrt{\omega^2 c^{-2} - k_x^2 - k_y^2}. \tag{2}$$

Two situations can arise: the first is when $\omega^2 c^{-2} > k_x^2 + k_y^2$, so that k_z is real and the corresponding term in equation 1 is a phase factor. Thus, the plane wave is propagating. On the other hand, if $\omega^2 c^{-2} < k_x^2 + k_y^2$, then k_z is imaginary and the resulting evanescent wave is exponentially decaying in the z direction. Therefore, a classic lens cannot recover evanescent waves when it is used to construct an image of the object. As a consequence, the image is imperfect due to

#6119 - $15.00 US Received 22 December 2004; revised 23 February 2005; accepted 23 February 2005

the loss of spatial information, corresponding to the high k_x and k_y values. The prediction by Pendry, which was not without controversy, was however that a slab of LHM can also amplify exponentially decaying evanescent waves [1]. The LHM lens *can* therefore include the evanescent fields coming from the object. The combination of focusing and amplification yields a perfectly reconstructed image, hence the term 'perfect lens'.

Though the concept of negative refraction is already a few decades old, experimental evidence of negative refraction by left handed material was presented just recently for the GHz range [3]. Here, the LHM slab was comprised of an engineered material using copper split ring resonators (SRRs) and wire strips. The combination of the SRRs and wires results in material with a negative μ and ε for a certain frequency band.

However, at optical frequencies in the range of several hundreds of THz, the constraint of having a negative ε as well as a negative μ cannot be fulfilled by any known natural material. A negative permittivity is attainable by metals near the plasma frequency, but then still $\mu \approx 1$. Scaling down SRRs to appropriate dimensions for visible light is unfortunately not feasible.

Pendry showed that there is a way out: in a quasi-electrostatic approach, the magnetic and electric fields can be considered decoupled and for P-polarized evanescent waves only the permittivity will be of relevance, regardless the value of μ. In other words, in a quasi-electrostatic case a negative permittivity suffices for creating a perfect lens. This imposes a new extra constraint on the detection scheme: for the electrostatic limit approach to be valid, all relevant dimensions must be such that retardation effects can be neglected. Thus, the entire object-lens-image system has to be much smaller than the wavelength of the light.

Absorption of light by the negative permittivity material will set an upper limit on the highest spatial frequency that can be mapped by the lens. As we will show, this does not impair the use of the negative permittivity lens for sub-wavelength imaging for k-values up to and including $\approx 10 \cdot 2\pi/\lambda$. We anticipate that, rather than being used for 'perfect' imaging purposes, the negative permittivity lens will find its use primarily in applications where sub-wavelength information in the form of evanescent waves is to be transferred and where only a discrete response is required, like in data storage and lithography. In these situations, the sensitivity of the lens to the polarization or, more useful in the near field, the actual E_x, E_y and E_z field components is less of an issue. Some features of the negative permittivity lens on the individual field components will be explored in this paper.

Up to now, much effort was put in numerically evaluating the optical properties of both LHM and negative permittivity material (NPM). Simulations indicate that the LHM slab indeed can amplify an incident evanescent wave. The transfer function $|\tau|$ for spatial frequencies k_x and k_y of a LHM slab can be near 1, where the highest spatial frequency that is imaged without distortion is limited by the absorption of the LHM slab [4, 5]. In the infrared regime, the applicability of the SRR/wire strips combination is investigated by the use of 2D transfer matrix method simulations [6]. Furthermore, the requirements for near-field amplification of exponentially decaying waves with a NPM lens are equal to the requirements for having a surface plasmon on the surface of the lens. It is therefore generally believed that surface plasmons are responsible for the reconstruction of the sub-wavelength features of the electric field [7].

Experiments that address the essential property of the NPM lens — amplification of evanescent waves and the recovery of high spatial detail — have also been performed. For example, AFM has been used to probe the height pattern of a developed film of photoresist, obtained after illuminating a mask with features the size of a few wavelengths down to the sub-wavelength scale in combination with a silver layer [8]. Far-field measurements also indicate the existence of enhanced transmissivity of evanescent waves through a silver film, where the evanescent waves are excited through surface roughness and the dipole radiation characteristics of the surface scatterers are analyzed [9]. However, direct evidence by measuring the local field of the

#6119 - $15.00 US Received 22 December 2004; revised 23 February 2005; accepted 23 February 2005

image and comparing it with the field of the object is still missing.

We propose a measurement scheme in which both the optical source as well as the detector have sub-wavelength dimensions: a combination of near-field scanning optical microscopy (NSOM) and single molecule detection (SMD) is capable of revealing the effect of the NPM lens on the individual components of the near-field and allows a direct comparison of the object and image fields. The single molecules will act as vectorial detectors of the fields so that not only the magnitude but also the direction of the reconstructed field can be determined. The scheme is therefore ideal for evaluating the imaging properties of the NPM lens.

2. A direct near-field method

The measurement scheme comprises the following ingredients: a sub-wavelength source of evanescent waves, hence our object in 'object-lens-image' terms, is a Focused Ion Beam (FIB) modified NSOM fiber probe [10]. A thin (∼20 nm) layer of metal, which is our negative permittivity material, is placed on a rigid polymer matrix. The metal layer will act as the lens. The polymer layer contains fluorescent molecules in a concentration that allows individual addressing of each molecule (typically 10^{-9} M). An accurate height control allows precise control over the distance between the NSOM probe and the sample [11]. The setup is schematically shown in Fig. 1.

As previously said, the single molecules will act as the required sub-wavelength detectors of the evanescent fields reconstructed by the negative permittivity lens. The fluorescence of a molecule directly reveals the local electromagnetic fields: the fluorescence intensity I_{fl} of the molecule is related as $I_{\mathrm{fl}} \propto \overline{E} \cdot \overline{\mu}$. Here, $\overline{E} \cdot \overline{\mu}$ is the vector dot product of the local electrical field $\overline{E}$ and the transition dipole of the molecule $\overline{\mu}$. Note that the molecule's fluorescence is sensitive to both the absolute value of the local electrical field as well as its orientation with respect to the dipole [12, 13, 14]. As a result, the full vectorial field coming from the sub-wavelength object can be explored.

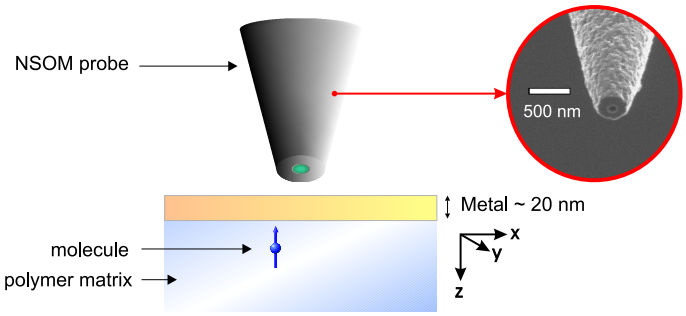

Fig. 1. Proposed near field set-up to evaluate the performance of the NPM lens. A NSOM probe is used as a sub-wavelength source of evanescent fields and is brought to within a few tens of nanometers away from the NPM lens by using shear-force feedback. The NPM lens is placed on a layer of a polymer matrix containing fluorescent molecules that are individually addressable and will act as sub-wavelength detectors sensitive to the vectorial nature of the local electromagnetic field. Shown in the red circle is a FIB image of a real NSOM probe with an aperture diameter of ∼ 100 nm.

The field components of a FIB modified NSOM fiber probe can be approximated by an analytical model formulated by Bethe and Bouwkamp, for probes having a low surface roughness [15, 16, 17]. For an aperture diameter of 100 nm, typical for a NSOM probe, a calculation based on the Bethe-Bouwkamp model is shown in Fig. 2 for a distance of 20 nm from the aperture.

#6119 - $15.00 US Received 22 December 2004; revised 23 February 2005; accepted 23 February 2005

Shown are, from left to right, the fields E_x, E_y and E_z respectively, where the subscript denotes the direction of the field. The planar wave used for the excitation is polarized in the x-direction as indicated by the E_{exc} symbol. The strongest field component near the aperture is E_x and it has the same direction as the polarization of E_{exc}. Orthogonal to E_x, but still in a plane parallel to the aperture, is E_y. The amplitude of this field is lower than the E_x field by more than a factor of seven. The last field present near the hole, E_z, is orthogonal to both E_x and E_y and it is only by a factor of two weaker than E_x,

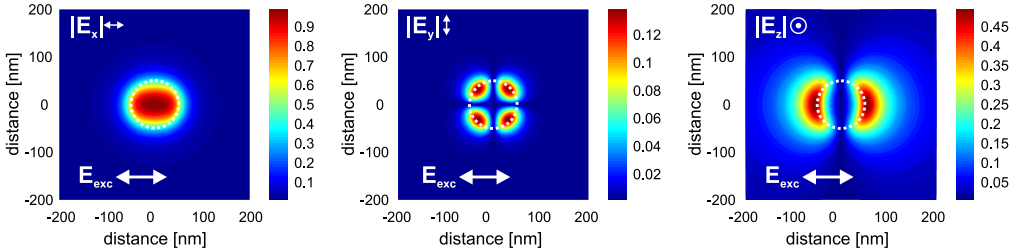

Fig. 2. False color representation of a Bethe-Bouwkamp calculation of the fields present at the end face of a near-field scanning probe with linearly polarized excitation light. Shown from left to right are the absolute values of E_x, E_y and E_z respectively. The field amplitudes are normalized to the maximum field amplitude of E_x. Aperture diameter = 100 nm, indicated by the white circle. Distance to the aperture = 20 nm and the wavelength = 514 nm. The rich variety of the field at the end face of the NSOM probe is evident.

Measurement schemes for mapping local fields employing local scatterers or fluorescent beads are unable to distinguish between the field components as they only detect the local intensity distribution. However, a single molecule is sensitive to both field amplitude *and* its direction. It therefore exclusively probes the local field in the direction of its transition dipole moment. By using differently oriented molecules it becomes possible to distinguish between the local field distributions in the various directions. The sensitivity of single molecules to various field directions is illustrated in Fig. 3(a). Experimental data depicted in Fig. 3(b) proves that single molecules actually map the local field of the NSOM probe.

Since for propagating waves, the NPM lens is not expected to enhance the image, the E_x field will be less suitable as an object since it also has propagating components (real k_z). In contrast, to probe the predicted lensing by a negative permittivity slab, measuring the E_z field is ideal to use as an object, because E_z is strongly evanescent. Nevertheless, both field components are evaluated in the simulations below to gain understanding of the near-field behavior of the NPM lens with respect to polarization.

3. Expected performance of the near-field set-up

In order to gain insight into the expected fields in our measurement scheme, we have modeled the measurement scheme presented here using a commercially available three-dimensional finite integration technique solver [18]. The schematic layout of the simulation model is shown in Fig. 4. The NSOM probe is modeled by a perfectly electrically conducting screen, with a circular aperture in it of a diameter of 100 nm. The NPM lens is described by a lossy Drude metal, modeled as

$$\varepsilon = \varepsilon_\infty - \frac{\omega_p^2}{(\omega^2 - i\omega\gamma)}. \tag{3}$$

#6119 - $15.00 US Received 22 December 2004; revised 23 February 2005; accepted 23 February 2005

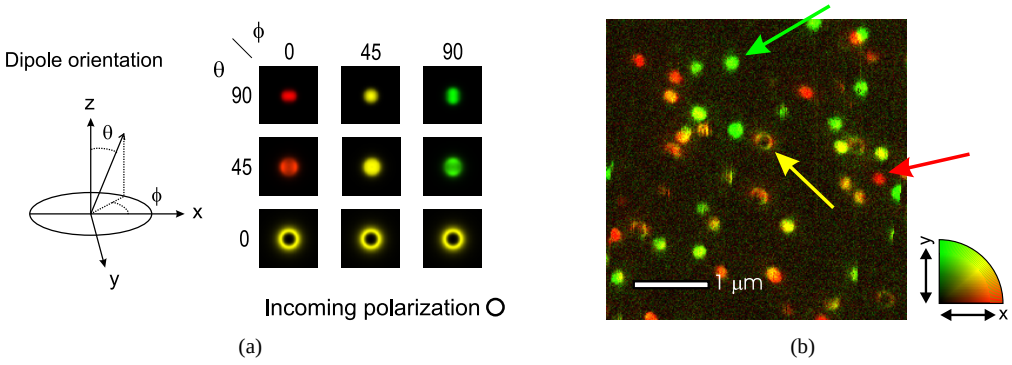

Fig. 3. (a) Mapping of the field components of a NSOM probe by a molecule with a dipole moment as indicated by θ and ϕ, using *circular* polarization. The E_x and E_y fields of the fluorescence light are color coded as red and green respectively. Because of the circular polarization of the exciting field, the E_z field is mapped as a donut-like shape. (b) Single molecule data obtained with NSOM using circularly polarized excitation light of 514 nm. The aperture diameter of the NSOM probe used in the measurement is 130 nm. The in-plane polarization of the emitted light is color-coded as in (a). A typical result for the three orthogonal directions are indicated by arrows. The red and green arrows point to molecules that have probed the E_x and E_y fields, respectively. A typical result for the E_z field is indicated by the yellow arrow. The E_z field is probed by an out-of-plane oriented ($\theta = 0$) molecule and the typical donut shape is retrieved. Clearly, the single molecule is capable of detecting the vectorial nature of the local electromagnetic field.

Here, ε_∞ is the dielectric response in the infinite frequency limit, ω_p is the plasma frequency and γ is the electron collision rate. In the following, all parameters are chosen such that the Drude response closely resembles that of silver [19]. No further assumptions are made. Specifically, no quasi-static approximations are made.

First, the situation without the NPM lens is regarded, where the simulation is basically a Bethe/Bouwkamp-like calculation of the electric field near a sub-wavelength hole. This three-dimensional calculation will be the reference pattern to which subsequent calculations will be compared. A plane wave ($\lambda_0 = 356$ nm) travels from the top of the simulation space towards the screen. The field components E_z and E_x that are induced at the aperture are evaluated along a line parallel to the screen at two distances from the aperture: at 10 nm away, corresponding to position 1 in Fig. 4, and at 40 nm away from the aperture, corresponding to position 2 in the same figure. Note that 10 nm is a typical probe-surface distance in near-field microscopy.

The normalized field magnitude of the E_x and E_z components at position 1, i.e. at 10 nm distance, is evaluated and is presented in Fig. 5. The result for this distance is represented by the blue line. Also without the lens, the normalized field magnitude at 40 nm distance, i.e., position 2, is evaluated and is represented by the green line. The field magnitudes are normalized to allow easy comparison of the shape of both fields. It is immediately visible that both the E_x and the E_z field components broaden with distance. Also, small lobes present in the E_x field at 10 nm from the screen are lost after a distance increase of 30 nm. The broadening is a direct consequence of Eq. 2 in case of an imaginary k_z: high spatial frequency, i.e., sub-wavelength, information and thus the 'sharpness' or confinement of the field distribution, decays with distance. The amount of broadening of the field distribution is however different for both the field components. For the E_x field, the full width at half the maximum (FWHM) increases by a fac-

#6119 - $15.00 US Received 22 December 2004; revised 23 February 2005; accepted 23 February 2005

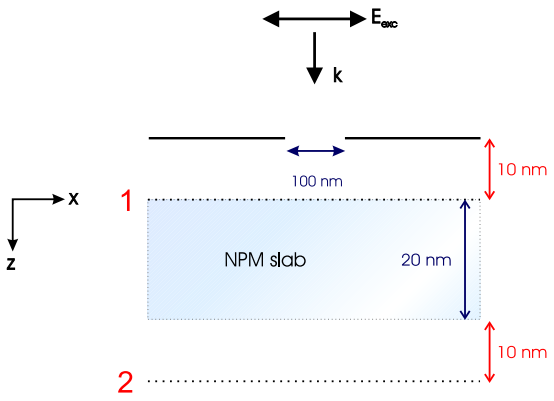

Fig. 4. Schematic layout of the simulation space (side view). A planar wave impinges a perfectly electrically conducting sheet, with a 100 nm circular aperture cut from it. The sheet with the aperture is our model for the NSOM probe, corresponding to a Bethe-Bouwkamp configuration. The E_z and E_x fields are evaluated at locations 1 and 2, both with and without a negative permittivity material slab. The results of these simulations are presented in Fig. 5.

tor of 1.2 for an increase in distance of 30 nm. The E_z field undergoes a significantly larger broadening over the same distance: the FWHM of a single lobe increases by a factor of 3.4.

Subsequently, while keeping the rest of the configuration the same, we introduce a 20 nm slab of negative permittivity material in the calculation. The Drude metal is driven at a frequency corresponding to the wavelength λ_0 in air, and exhibits a permittivity $\varepsilon = -1 + 0.4i$ at that frequency. The fields are again evaluated at position 2 and plotted in Fig. 5 as red curves.

Clearly, the results obtained by the simulations show that the slab of negative permittivity material recovers the sharpness of the fields at position 2 behind the lens. For the E_x component, the FWHM of the red curve is nearly identical to the FWHM of the green curve, suggesting some focusing. Furthermore, some of the detail in the form of lobes that had been lost without the lens is reconstructed. Shoulders appear in the pattern more than 100 nm away from the center. These shoulders might be attributed to resonances in the transfer function of the NPM slab, caused by deviations from the ideal lossless and quasi-static situation [20]. For the E_z field, the red curve is much more confined when compared to the green curve. We can define the relative effect on the FWHM as the ratio of the width of the field at 40 nm without the NPM slab to the width of the field at 40 nm *with* NPM slab ($\mathrm{FWHM}_{40\ \mathrm{nm}}/\mathrm{FWHM}_{40\ \mathrm{nm,lens}}$). This ratio is for the E_x field 1.3 whereas $\mathrm{FWHM}_{40\ \mathrm{nm}}/\mathrm{FWHM}_{40\ \mathrm{nm,lens}}$ for a single lobe of E_z is 1.9. The E_z field is ideal to probe the performance of the lens, because of two reasons. The first is that the FWHM of the E_z field is much more sensitive to distance than the E_x field. A small change in distance therefore has a much higher impact on the shape of the pattern when compared to the E_x field which makes the FWHM of the E_z pattern a good marker for the distance. Second, the influence of the lens on the FWHM of the pattern of E_z is larger than the influence on the FWHM of the pattern of E_x. This allows a more accurate experimental determination of the lens with the pattern of the E_z field.

These simulations clearly demonstrate the effect of decay of evanescent fields on the sharpness of the pattern: the image sharpness is strongly distance dependent, where steep edges get smoothed with distance. Hence, we conclude that the image obtained by the mapping of the single molecule will be dependent on both the distance of the molecule to the aperture as well as the performance of the NPM lens. The distance between the NSOM probe and the molecule,

#6119 - $15.00 US Received 22 December 2004; revised 23 February 2005; accepted 23 February 2005

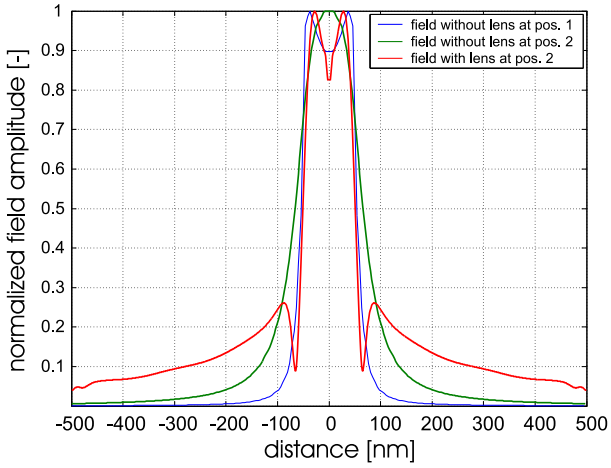

(a) E_x field magnitude

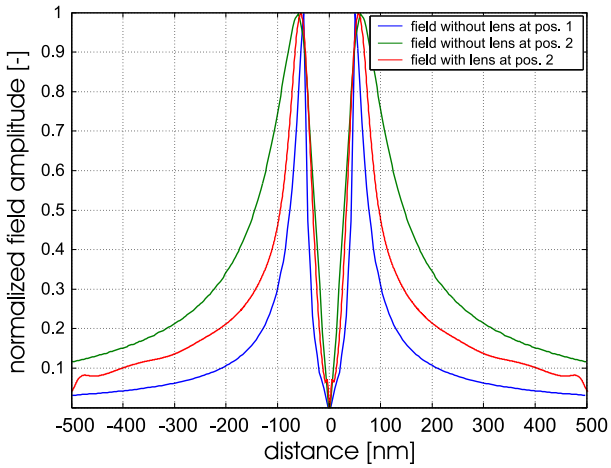

(b) E_z field magnitude

Fig. 5. Simulation results. Shown are the components $|E_x|$ and $|E_z|$ in Fig. (a) and (b) respectively. The normalized magnitude of the field components is plotted, evaluated at position 1 *(green curve)* and at position 2 *(blue curve)* as displayed in Fig. 4, both for the slab-less situation. Clearly visible is the broadening of the field with distance. *Red curve:* the NPM slab is inserted and the magnitude of the fields is evaluated once again at position 2. The resulting field magnitudes are more confined and show more detail than their counterparts without the lens, the green curves.

combined with the measured evolution of image sharpness with distance, allows for a direct comparison between patterns characteristic for excitation with circularly polarized light with and without a lens present so that the imaging properties of the NPM lens can be addressed.

4. Measured evolution of $|E_z|^2$ with height

Data on the evolution of the single molecule pattern as a function of distance is needed to be able to compare image sharpness with and without a NPM slab present. Here, we focus on

#6119 - $15.00 US Received 22 December 2004; revised 23 February 2005; accepted 23 February 2005

the detection of E_z for reasons made clear in the previous section. Note that I_{fl} of a vertically oriented molecule is proportional to $|E_z|^2$. Figure 6 presents the mapping of the height dependence of the $|E_z|^2$ field using the fluorescence of a vertically oriented molecule that exhibits the donut-like excitation pattern. From this data, the full width at half the maximum as a function of height can be extracted, by performing a cross-section through the pattern. Taking the center of the pattern as the origin, this results in a radial distribution of the intensity in fluorescence photon counts. To improve on the signal to noise ratio, for each probe-sample distance all pixels lying on a circle with a certain radius from the center of the pattern are integrated over 2π. The result is then divided by the number of pixels, which yields the average number of counts for a certain radius. This process is repeated for all radii.

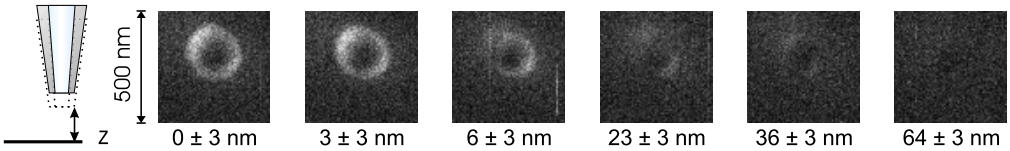

Fig. 6. Intensity-map by a single molecule of the E_z field as a function of probe-sample distance. The molecule is DiIC_{18} and is excited with circularly polarized light of 514 nm (in vacuum). The NSOM probe has an aperture diameter of 130 nm. Below each image the respective distance is indicated, where a distance of zero nm equals the 'in-contact' situation. The fast decay of the field intensity with distance is evident, as well as the broadening of the pattern as is expected from the simulations.

Figure 7 shows the radial distribution of the fluorescence counts as a function of probe-sample distance *(solid lines)*. Also shown are calculated radial distributions *(dotted lines)*. For these calculations the experimental data for the 'in-contact' case are fitted with the Bethe-Bouwkamp model, with the 'in-contact' probe-sample distance, the aperture of the NSOM probe, the background intensity and a scaling factor to correct for the input power as the free parameters. The result is the blue dotted line in Fig. 7. We find for the NSOM aperture diameter 154 nm, for the 'in-contact' distance 41 nm and for the background intensity 44 counts. The subsequent calculations for the other heights contain no free parameters and have only the measured height as input. The calculated theoretical curves are in good agreement with the measured data.

Furthermore, from Fig. 7 we can directly map image sharpness to distance between the NSOM probe and the single molecule. There are various ways to do this, but for reasons explained in the previous section the FWHM is a very suitable candidate. The FWHM versus distance of the data in Fig. 7 is shown in Fig. 8. Clearly, the measured data is in good agreement with the theoretical curve. The single molecule thus is able to map the FWHM of the E_z pattern as a function of distance, making the decrease of image sharpness with distance directly visible.

The influence of the NPM lens is that the FWHM of the pattern, as imaged by the single molecule, is less than can be expected given the total distance from the aperture. Therefore also the distance-dependency is different from what can be expected. Measuring the distance-dependent pattern of the E_z field with a NPM lens present will immediately reveal this non-standard behavior. A direct comparison with the E_z pattern without a lens will then unravel the imaging properties of the NPM lens.

5. Conclusion

We have presented a novel method that can directly evaluate the performance of a negative permittivity slab at optical frequencies. The usefulness of near-field scanning optical microscopy

#6119 - $15.00 US Received 22 December 2004; revised 23 February 2005; accepted 23 February 2005

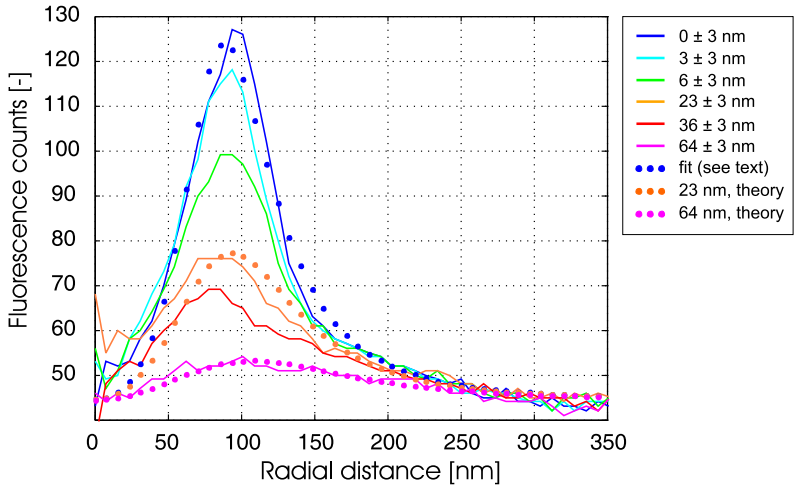

Fig. 7. Measured radial distribution of $|E_z|^2$ as a function of distance. The origin maps to the center of the donut-shaped image in Fig. 6. Next to the measured data, a fit of the data with the Bethe-Bouwkamp model is also displayed (*blue dots*). Based on the fit, the theoretical curves for distances of 23 and 64 nm are calculated (*orange* and *purple dots* respectively). The broadening of the pattern with distance is apparent.

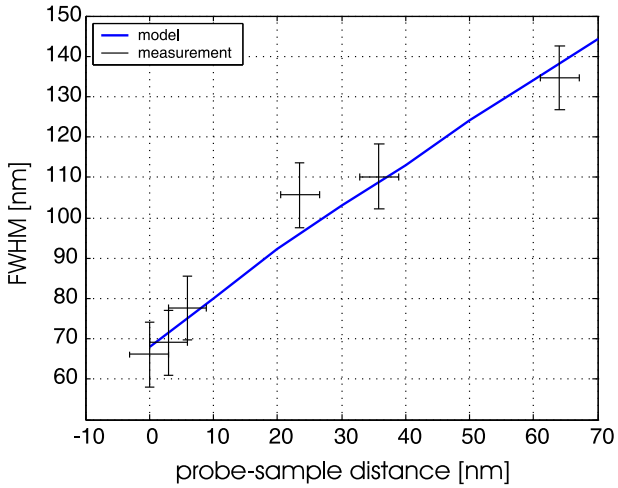

Fig. 8. Measured FWHM of the $|E_z|^2$ pattern in Fig. 7 as a function of distance. The measured data is obtained from Fig. 7 and the theoretical curve is obtained from the Bethe-Bouwkamp model. The model and the data are in good agreement, showing that the use of the FWHM of the E_z field as a quantitative means to investigate the influence of the negative permittivity material lens on image formation is very well feasible.

#6119 - $15.00 US Received 22 December 2004; revised 23 February 2005; accepted 23 February 2005

combined with single molecule detection is confirmed through our simulations. The simulations, which incorporate a Drude model realistic for silver, show that the negative permittivity slab will enhance the detail of the local field. Absorption limits the total enhancement of the image by the NPM slab, but nevertheless for the FWHM specifically the influence of the lens on the E_z field is large: a reduction of the feature broadening by a factor of 1.9 is found. The calculations show the necessity of a vector detector, like a single molecule, for the evaluation.

Through single molecule detection, we have measured how the E_z field evolves with height. The measurements show the feasibility to use the near-field distance-dependency of the E_z field as a marker for the reconstruction of the E_z field by a NPM lens.

#6119 - $15.00 US Received 22 December 2004; revised 23 February 2005; accepted 23 February 2005